American Mineralogist, Volume 80, pages 923–929, 1995

Orthopyroxene from the Serra de Magé meteorite: Structure refinement and estimation of *C*2/*c* pyroxene contributions to apparent *Pbca* diffraction violations

M. Chiara Domeneghetti
CNR, Centro di Studio per la Cristallochimica e la Cristallografia, % Dipartimento di Scienze della Terra, Università di Pavia, Via Abbiategrasso 209, 27100 Pavia, Italy
G. Mario Molin, Marilena Stimpfl
Dipartimento di Mineralogia e Petrologia, Università di Padova, Corso Garibaldi 37, 35100 Padua, Italy
Mario Tribaudino
Dipartimento di Scienze Mineralogiche e Petrologiche, Università di Torino, Via Valperga Caluso 35, 10125 Turin, Italy

Abstract

Transmission electron microscopy (TEM) of microstructures in the orthopyroxene of the Serra de Magé cumulate eucrite shows augite lamellae thicker than 500 Å, irregularly spaced within the orthopyroxene matrix and parallel to (100), with $\mathbf{a}^*_{Opx} \equiv \mathbf{a}^*_{Aug}$, $[101]^*_{Opx} \equiv \mathbf{c}^*_{Aug}$, and $\mathbf{b}^*_{Opx} \equiv \mathbf{b}^*_{Aug}$. Streaking along $\mathbf{a}^*$ owing to stacking disorder was observed in selected-area electron diffraction (SAD) patterns. Slabs of clinopyroxene were observed, but no Guinier-Preston zones were detected. Single-crystal X-ray diffraction (XRD) data were collected and structure refinements completed in space group *Pbca*, converging to $R_{obs} = 2.81$ and 5.17% for the two samples. Because of the presence of some $0kl$ forbidden reflections with $k = 2n + 1$ and $l = 4n + 2$, structure refinement was attempted in space group $P2_1ca$, as suggested by previous studies, and in space groups $P12_1/c1$ and $P112_1/a$, as suggested by the Laue symmetry of the reflections, which is $2/m$ rather than *mmm*. However, the high residual indices *R* and the anomalous values of many displacement parameters and bond distances did not support the lower-symmetry space groups. The violations of the extinction conditions of the *Pbca* space group and the monoclinic symmetry of the reflections are due to overlap of reflections from the *C*2/*c* augite lamellae. From the intensity of the reflections forbidden in *Pbca* space group, the calculated augite content ranges from approximately 4 to 12%.

Introduction

The Serra de Magé meteorite is a cumulate eucrite containing plagioclase and pyroxene. A detailed investigation of textural relations in the Serra de Magé meteorite (Harlow et al., 1979) showed that the pyroxene crystallized as pigeonite, which exsolved (001) augite lamellae and then inverted to hypersthene with thin (100) augite. The presence of $0kl$ reflections with $k = 2n + 1$, forbidden by the *b*-glide plane in the *Pbca* space group, suggested that the Serra de Magé hypersthene has the lower $P2_1ca$ symmetry previously described for lunar pyroxenes (Smyth, 1974, 1975; Steele, 1975). However, Sasaki et al. (1984) proposed the following alternative explanations for the forbidden reflections that do not involve pyroxene with the $P2_1ca$ space group: (1) Type I: coexisting *C*2/*c* clinopyroxene exsolved on (100); (2) Type II: diffuse streaks from upper levels; and (3) Type III: multiple diffraction effects. In particular, Sasaki et al. (1984) considered the Serra de Magé pyroxene as a "simple case of Type I cpx diffraction." More recently, Luo et al. (1992) confirmed the occurrence of space group $P2_1ca$ in two terrestrial orthopyroxenes by TEM observations during heating of a hypersthene. The disappearance of all $(0kl)$ diffraction spots with *k* odd at 900 °C suggested to these authors that a reversible $P2_1ca \rightarrow Pbca$ phase transformation could occur at this temperature.

The aim of the present study is to determine the true symmetry of the Serra de Magé orthopyroxene. In particular, the availability of two single crystals of good quality has allowed us to test the alternative hypothesis for the $P2_1ca$ symmetry by performing structure refinements that have never been attempted on this sample.

Experimental methods

Samples SDM N.13 and SDM N.7 were obtained from a fragment of the Serra de Magé eucrite (meteorite collection of Dipartimento di Scienze della Terra, Università di Modena, Italy). They are the only single crystals found that are suitable for X-ray analysis; because they are still under investigation, we have not used them for TEM or microprobe analysis. TEM analysis was performed on separate orthopyroxene grains selected from

0003–004X/95/0910–0923$02.00

TABLE 1. Electron microprobe analysis of Serra de Magé orthopyroxene

Chemical composition of host + augite lamellae*			
Oxide	wt%	Atoms per formula unit (based on six O atoms)	
SiO_2	52.73(48)	Si	1.995(8)
Al_2O_3	0.37(5)	$^{[4]}Al$	0.005(2)
		$^{[6]}Al$	0.011(7)
FeO	25.03(53)	Fe^{2+}	0.792(21)
MgO	19.68(21)	Mg	1.110(11)
MnO	0.85(5)	Mn	0.027(2)
TiO_2	0.16(1)	Ti	0.005(1)
Cr_2O_3	0.19(4)	Cr	0.006(1)
CaO	0.96(10)	Ca	0.039(4)
Sum	99.97	Sum	3.990

Note: standard deviations are in parentheses.
* Average of 16 spots by the EMPA analysis.

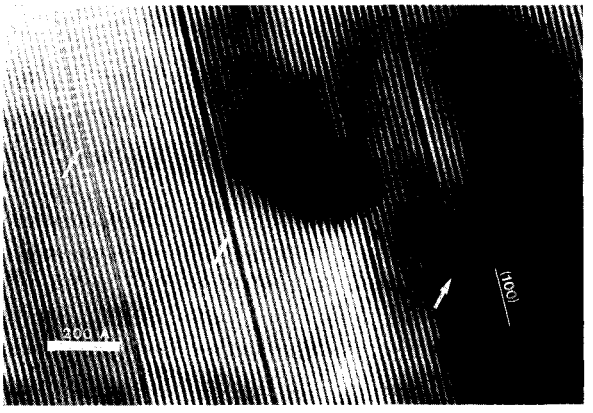

Fig. 1. High-resolution transmission electron microscope image of orthopyroxene. Fringes parallel to (100) are shown. Arrows indicate stacking faults within the orthopyroxene matrix.

the same small fragment of the meteorite. Electron microprobe analysis was performed on a polished thin section of the meteorite.

TEM analysis

The samples were prepared by crushing composite grains of orthopyroxene in an agate mortar. Samples were dispersed on a Cu grid covered with a holey carbon film. The grain size obtained by crushing was a few micrometers. The grid was not subsequently coated. TEM analysis was performed at 120 kV using a Philips CM12 microscope equipped with an energy dispersive (EDS) analytical system and a double-tilt stage. Analytical electron microscope analyses were performed with minimum spot size (400 Å). Theoretical k factors were used to reduce the data by the Cliff-Lorimer thin-film approximation.

Electron microprobe analysis

Electron microprobe analysis (EMPA) was conducted on a thin polished section with a CAMECA CAMEBAX electron microprobe in wavelength-dispersive (WDS) mode, operating with a fine-focused beam (~1 μm) at 15 kV and using a 15 nA sample current, with peak and background counting times of 20 s. The following synthetic end-member mineral standards were used: diopside for Mg; ferrosilite for Fe; wollastonite for Si and Ca; chromite for Cr; corundum for Al; albite for Na; and $MnTiO_3$ for Mn and Ti. X-ray counts were converted into oxide weight percentages using the PAP correction program provided by CAMECA. The average of 16 spots selected from three orthopyroxene crystals represents the bulk composition of combined host orthopyroxene + augite lamellae (Table 1).

TABLE 2. Cell parameters and refinement data (space group *Pbca*)

	OPX SDM N.13, natural	OPX SDM N.7, heated 47.66 h at 900 °C
a (Å)	18.316(13)	18.320(18)
b (Å)	8.907(7)	8.917(7)
c (Å)	5.218(6)	5.219(6)
V (Å^3)	851.2	852.6
No. of ind. refl.	1247	1252
R_{sym} (%)	6.3	7.1
No. of I_{obs}	868	845
R_{obs} (%)	2.81	5.17
R_{tot} (%)	5.20	9.12
M.a.n. M1	13.46(16)	15.25(31)
M.a.n. M2	22.18(18)	20.31(34)

Note: R_{sym} refers to the agreement among the intensities of the equivalent reflections hkl, $\bar{h}kl$, $h\bar{k}l$, and $\bar{h}\bar{k}l$. $R_{sym} = \Sigma_{hkl}(I_{hkl} - \bar{I})/\Sigma_{hkl}\bar{I}$, where $\bar{I} = (I_{hkl} + I_{\bar{h}kl} + I_{h\bar{k}l} + I_{\bar{h}\bar{k}l})/4$. I_{obs} = reflections with $I \geq 3\sigma_I$. R_{obs} and R_{tot} are the final conventional discrepancy indices expressed as $\Sigma||F_o| - |F_c||/\Sigma|F_o|$. M.a.n. = mean atomic number.

X-ray data collection

Two orthopyroxene single crystals were selected for X-ray diffraction analysis. Opx SDM N.13 is a natural, untreated crystal approximately 170 × 180 × 200 μm; Opx SDM N.7, approximately 180 × 310 × 330 μm, was previously used for heating experiments in a thermodynamic study and therefore has a more disordered Fe^{2+} distribution.

Single-crystal X-ray intensity data were obtained using a Philips PW 1100 four-circle automated diffractometer and graphite monochromatized Mo$K\alpha$ radiation (λ = 0.71073 Å). Net X-ray diffraction intensities were determined by measuring step-scan profiles and analyzing them by the Lehmann and Larsen (1974) σ_I/I method as modified by Blessing et al. (1974). The equivalent reflections hkl, $\bar{h}kl$, $h\bar{k}l$, and $\bar{h}\bar{k}l$ were measured up to $\theta \leq 30°$ in the ω-scan mode. The intensities were corrected for absorption using the semiempirical method of North et al. (1968), and the values of equivalent reflections were averaged; the resulting discrepancy factors $R_{sym} = \Sigma_{hkl}(I_{hkl} - \bar{I})/\Sigma_{hkl}\bar{I}$, where $\bar{I} = (I_{hkl} + I_{\bar{h}kl} + I_{h\bar{k}l} + I_{\bar{h}\bar{k}l})/4$, were 6.3 and 7.1%.

The cell dimensions were determined using a locally improved version (Cannillo et al., 1983) of the Philips LAT routine and are reported in Table 2.

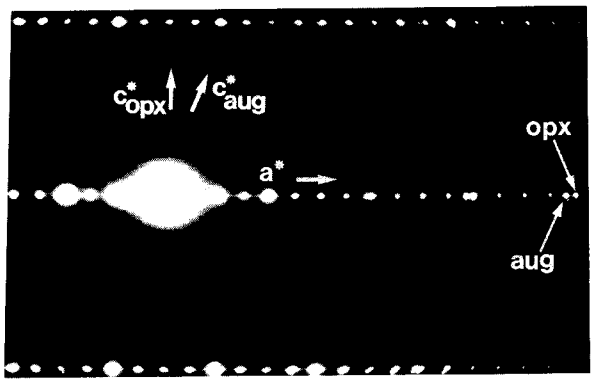

Fig. 2. Selected area diffraction (SAD) pattern corresponding to Fig. 3. Note the splitting (arrows) along **a*** owing to the superimposition of augite and orthopyroxene diffraction maxima and the streaking along **a*** owing to stacking disorder.

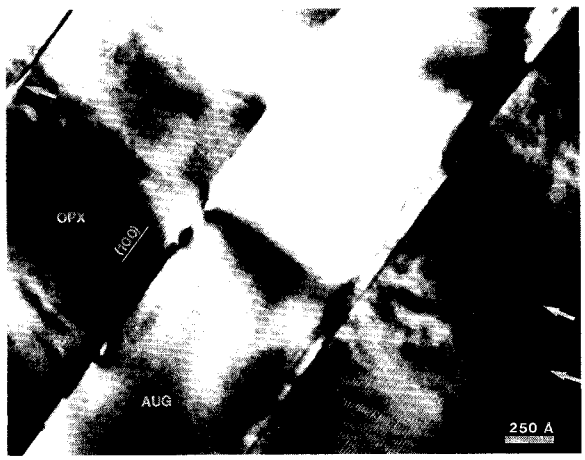

Fig. 3. Augite lamella within orthopyroxene matrix. Stacking faults appear at the upper left and lower right (arrows), and there are ledges at the interface between clinopyroxene and orthopyroxene. Bright-field image.

Results

TEM textures

In the sample examined, separate grains of both orthopyroxene and Ca-rich clinopyroxene were present, with orthopyroxene being most abundant. In orthopyroxene, stacking faults were observed parallel to (100), with a repeat along [100] larger than 500 Å (Fig. 1). They are responsible for the slight streaking observed along **a*** (Fig. 2). We suggest that these faults may have formed as a result of weak shock. No Guinier-Preston zones were observed. In Harlow et al. (1979), optical and electron microscopy revealed four types of augite exsolution within orthopyroxene, three of them >5 μm in width. In the present study, only the smallest type of exsolution lamellae (A2 lamellae in Harlow et al., 1979) was observed within orthopyroxene (Fig. 3). It is possible that the other types of exsolution lamellae are too coarse to be observed in orthopyroxene grains of the size examined here; they are probably found in the sample as separate grains of Ca-rich clinopyroxene. A2 exsolution lamellae are uncommon and irregularly spaced. They are >500 Å in thickness and are parallel to (100), with $\mathbf{a}^*_{Opx} \equiv \mathbf{a}^*_{Aug}$, $[101]^*_{Opx} \equiv \mathbf{c}^*_{Aug}$, and $\mathbf{b}^*_{Opx} \equiv \mathbf{b}^*_{Aug}$. Ledges at the augite-orthopyroxene interface were observed. Table 3 gives analytical electron microscopy (AEM) analyses for orthopyroxene in an area free of stacking faults and for an A2 clinopyroxene lamella within the orthopyroxene host.

Structure refinement in *Pbca*

Initially the refinement was performed in the space group *Pbca*, without chemical constraints, using a locally modified version of the least-squares program ORFLS (Busing et al., 1962) and starting with the positional and displacement parameters of an orthopyroxene of similar composition. The program allows the assignment of two scattering curves, f_1 and f_2, to each site and refinement of the occupancy factors x(f) with the constraint $x(f_1) + x(f_2) = 1$. The sum $x(f_1)N_1 + x(f_2)N_2$, where N_1 and N_2 are the number of electrons referring to f_1 and f_2, provides the mean atomic number at the site. The atomic scattering curves were taken from the *International Tables for X-ray Crystallography* (Ibers and Hamilton, 1974) and from Tokonami (1965). The ionization states used were 2.0+ for Si, Mg, and Fe, and 1.5− for O. There were 868 and 845 reflections, with $I \geq 3\sigma_I$, considered to be observed and used for the refinement with unit weights. In addition to the scale factor and extinction coefficient, 30 atomic positions and anisotropic displacement parameters were refined, varying all parameters simultaneously. No correlation >0.65 was observed. For the two crystals, refinement converged to residual indices R_{obs} of 2.81 and 5.17%, respectively.

The final difference-Fourier maps were featureless. Selected interatomic distances and angles for the two crystals are reported in Table 4. The final positional and displacement parameters are reported in Table 5. The observed and calculated structure factors (Tables 6 and 7) have been deposited.[1] Because the chemical analyses were not made on the same crystals used for the X-ray study, and because they reflect the composition of the host + augite lamellae, the site populations for both sam-

[1] A copy of Tables 6 and 7 may be ordered as Document AM-95-598 from the Business Office, Mineralogical Society of America, 1015 Eighteenth Street NW, Suite 601, Washington, DC 20036, U.S.A. Please remit $5.00 in advance for the microfiche.

Table 3. Analytical electron microscope analyses of Serra de Magé orthopyroxene

	EDS analysis of Opx in a lamella-free zone*	EDS analysis of Cpx lamella within Opx*
Si	2.00	2.00
Al	0.02	0.03
Fe^{2+}	0.84	0.35
Mg	1.07	0.76
Mn	0.03	—
Ca	0.03	0.88
Sum	3.99	4.02

* Normalized to two Si atoms per formula unit.

TABLE 4. Selected interatomic distances (Å) and angles (°) (space group *Pbca*)

	OPX SDM N.13, natural	OPX SDM N.7, heated 47.66 h at 900 °C
SiA-O1A	1.611(3)	1.607(6)
SiA-O2A	1.599(3)	1.592(6)
SiA-O3A	1.636(3)	1.621(6)
SiA-O3A	1.657(3)	1.673(6)
⟨SiA-O⟩	1.626(3)	1.623(6)
O3A-O3A-O3A	165.86	164.77
SiB-O1B	1.623(3)	1.622(6)
SiB-O2B	1.599(3)	1.590(6)
SiB-O3B	1.663(3)	1.655(6)
SiB-O3B	1.668(3)	1.681(6)
⟨SiB-O⟩	1.638(3)	1.637(6)
O3B-O3B-O3B	144.27	143.74
M1-O1A	2.037(3)	2.065(6)
M1-O1A	2.144(3)	2.149(6)
M1-O1B	2.166(3)	2.170(6)
M1-O1B	2.065(3)	2.088(6)
M1-O2A	2.035(3)	2.034(6)
M1-O2B	2.066(3)	2.067(6)
⟨M1-O⟩	2.085(3)	2.095(6)
M2-O1A	2.161(3)	2.151(6)
M2-O1B	2.121(3)	2.109(6)
M2-O2A	2.053(3)	2.069(6)
M2-O2B	2.005(3)	2.011(6)
M2-O3A	2.374(3)	2.363(6)
M2-O3B	2.531(3)	2.520(6)
⟨M2-O⟩	2.207(3)	2.204(6)

Note: standard deviations are in parentheses.

ples (see Table 8) were calculated using the equations of Domeneghetti et al. (1995), which express the atomic fractions at the structural sites as a function of cell parameters, atomic positions, and mean atomic numbers of M1 and M2 sites.

The rather high discrepancy factors R_{obs} for the *Pbca* structure refinements, in particular that of sample SDM N.7, and the presence of microstructures revealed by TEM analysis induced us to check the systematic extinctions. This showed the presence of reflections violating the systematic absence $k = 2n + 1$ on $(0kl)$ for the b-glide plane, thus confirming the previous observations of Harlow et al. (1979) and Sasaki et al. (1984) on Serra de Magé orthopyroxene. In both crystals, the reflections 032, 052, 072, 016, and 056 have $I \geq 3\sigma_I$. Intensity measurements at different values of ψ angle show that these reflections are not due to multiple diffraction, and analysis of the diffraction profiles excludes the possibility of overlap by diffuse streaks from other levels. We also recorded other reflections, with $I \geq 3\sigma_I$, forbidden by *Pbca* symmetry: 030, 13 0 0, 17 0 0, 21 0 0, and 21 5 0. This latter set of reflections has been recorded in several terrestrial and synthetic orthopyroxenes. Because these reflections are not a problem specific to the Serra de Magé orthopyroxene, we do not consider them here.

Structure refinement in $P2_1ca$

Because of the presence of reflections violating b-glide symmetry, structural refinement was attempted in the noncentrosymmetric space group $P2_1ca$, even if the magnitudes and orientations of thermal vibration ellipsoids that resulted from *Pbca* refinement did not suggest this approach. Information on the refinements in $P2_1ca$ are reported in Table 9. The reflections with $I \geq 3\sigma_I$ were considered to be observed. Least-squares refinements were conducted using the atomic positions of the independent atoms in the *Pbca* space group, together with those of their corresponding centrosymmetric atoms, and the same cell origin as in *Pbca*. Isotropic refinement was initiated by applying small shifts, in various directions, to some atomic positions of the second set of atoms. The atomic positions and the isotropic displacement factors of the

TABLE 5. Atomic positional parameters and displacement parameters (space group *Pbca*)

	x	y	z	β_{11}	β_{22}	β_{33}
			OPX SDM N.13, natural			
SiA	0.27149(6)	0.34060(12)	0.05180(20)	0.00044(3)	0.00135(11)	0.00294(31)
SiB	0.47403(5)	0.33660(12)	0.79535(20)	0.00047(3)	0.00154(12)	0.00219(32)
O1A	0.18355(14)	0.33731(34)	0.04361(52)	0.00046(7)	0.00239(30)	0.00322(82)
O1B	0.56266(14)	0.33632(33)	0.79552(54)	0.00042(7)	0.00255(31)	0.00364(82)
O2A	0.31117(15)	0.50053(32)	0.05332(54)	0.00069(7)	0.00192(31)	0.00466(86)
O2B	0.43402(15)	0.48555(33)	0.69789(53)	0.00070(7)	0.00249(32)	0.00455(85)
O3A	0.30233(15)	0.23184(33)	−0.17642(59)	0.00060(7)	0.00273(32)	0.00635(93)
O3B	0.44739(15)	0.20280(32)	0.59356(57)	0.00062(7)	0.00280(33)	0.00649(97)
M1	0.37540(7)	0.65459(12)	0.87426(22)	0.00056(3)	0.00177(13)	0.00263(38)
M2	0.37797(4)	0.48308(7)	0.36794(13)	0.00062(2)	0.00245(8)	0.00259(22)
			OPX SDM N.7, heated			
SiA	0.27178(10)	0.34044(23)	0.05067(40)	0.00035(5)	0.00100(21)	0.00544(60)
SiB	0.47383(10)	0.33640(23)	0.79521(38)	0.00044(5)	0.00132(21)	0.00450(64)
O1A	0.18414(27)	0.33775(63)	0.03730(98)	0.00031(12)	0.00196(55)	0.00475(158)
O1B	0.56235(26)	0.33755(61)	0.79219(99)	0.00021(12)	0.00280(57)	0.00449(160)
O2A	0.31098(28)	0.49976(62)	0.04844(104)	0.00038(13)	0.00262(60)	0.00658(166)
O2B	0.43401(29)	0.48420(63)	0.69768(104)	0.00054(14)	0.00341(63)	0.00609(176)
O3A	0.30222(28)	0.23043(62)	−0.17242(111)	0.00060(13)	0.00300(62)	0.00629(167)
O3B	0.44755(29)	0.20209(58)	0.59672(107)	0.00067(14)	0.00262(60)	0.00584(179)
M1	0.37558(10)	0.65406(20)	0.87255(36)	0.00044(5)	0.00145(22)	0.00435(67)
M2	0.37776(8)	0.48319(16)	0.36681(27)	0.00057(4)	0.00271(17)	0.00439(49)

Note: standard deviations are in parentheses.

TABLE 8. Site populations of Serra de Magé orthopyroxenes

Site population*		Opx SDM N.13, natural	Opx SDM N.7, heated 47.66 h at 900 °C
T	Si	2.000	2.000
M1	Fe^{2+} + Mn	0.104(5)	0.232(11)
	Mg	0.896(5)	0.768(11)
M2	Fe^{2+} + Mn	0.703(6)	0.570(12)
	Mg	0.254(6)	0.387(12)
	Ca	0.043	0.043

Note: standard deviations are in parentheses.
* According to Domeneghetti et al., 1995.

two sets of atoms and the scale factor and extinction coefficient were varied alternatively to avoid correlation effects. The lowest R indices obtained in the isotropic refinements were 4.37% for Opx SDM N.13 and 6.20% for Opx SDM N.7. Least-squares refinements with anisotropic displacement parameters reduced the R_{obs} index to 2.69 and 5.27%, respectively. At this point a full-matrix refinement was attempted. However, because the results worsened using this procedure, we have ignored them here. With respect to the refinement in *Pbca,* refinement in $P2_1ca$ gives an R index slightly higher for sample Opx SDM N.7 and lower for Opx SDM N.13. This improvement in the value of the R_{obs} index is not statistically significant when evaluated with Hamilton's test (Hamilton, 1965). Moreover, the refinements in the noncentrosymmetric space group are not considered reliable for the following reasons: (1) after every cycle of the least-squares refinement, the isotropic displacement parameters of many O atoms were negative; (2) the final values of many cation-O distances are anomalous. In particular, for samples Opx SDM N.13 and Opx SDM N.7, ⟨SiA-O⟩ [1.605(5), 1.601(9) Å] and ⟨SiB′-O⟩ [1.618(5), 1.620(10) Å] are too short, and ⟨SiA′-O⟩ [1.647(5), 1.645(10) Å] is too long for tetrahedra fully occupied by Si. (SiA′ and SiB′ refer to atoms of the second set, which were equivalent to SiA and SiB in the centrosymmetric space group.) Moreover, ⟨SiB-O⟩ values of 1.659(5) and 1.657(11) Å indicate a high $^{[4]}$Al content, which is not supported by the results of the AEM analysis.

TABLE 5.—*Continued*

β_{12}	β_{13}	β_{23}	B_{eq} (Å²)
	OPX SDM N.13, natural		
−0.00013(5)	−0.00001(7)	−0.00008(18)	0.44
0.00014(5)	0.00009(7)	0.00001(17)	0.45
−0.00010(12)	0.00033(20)	0.00016(49)	0.57
0.00011(13)	−0.00036(20)	0.00031(48)	0.59
−0.00020(13)	−0.00058(21)	0.00004(48)	0.68
0.00032(13)	−0.00019(21)	0.00076(49)	0.74
0.00001(13)	0.00036(23)	−0.00239(48)	0.79
−0.00003(13)	−0.00014(24)	−0.00234(48)	0.81
0.00000(6)	−0.00015(9)	0.00015(19)	0.53
−0.00012(3)	−0.00048(5)	−0.00008(11)	0.63
	OPX SDM N.7, heated		
−0.00020(9)	−0.00014(14)	0.00006(35)	0.46
0.00021(9)	0.00028(14)	0.00020(32)	0.50
−0.00008(24)	−0.00009(37)	0.00090(90)	0.52
0.00011(23)	−0.00009(37)	0.00101(88)	0.55
−0.00036(24)	−0.00045(38)	0.00053(96)	0.69
0.00020(24)	−0.00002(41)	0.00020(92)	0.82
−0.00038(25)	0.00063(45)	−0.00173(90)	0.81
0.00005(23)	−0.00002(46)	−0.00273(87)	0.79
−0.00003(9)	0.00008(14)	0.00008(29)	0.51
−0.00010(7)	−0.00033(11)	−0.00006(22)	0.70

TABLE 9. Refinement data (space groups $P2_1ca$, $P12_1/c1$, and $P112_1/a$) for Serra de Magé orthopyroxenes

	No. of ind. refl.	R_{sym} (%)	No. of I_{obs}	R_{obs} (%)	R_{tot} (%)
	P*2₁*ca				
OPX SDM N.13, natural	1287	6.3	874	2.69	5.60
OPX SDM N.7, heated 47.66 h at 900 °C	1292	7.1	854	5.27	9.45
	***P*12₁/*c*1**				
OPX SDM N.13, natural	2624	4.4	1732	4.15	6.55
OPX SDM N.7, heated 47.66 h at 900 °C	2676	1.6	1924	9.51	11.36
	P*112₁/*a				
OPX SDM N.13, natural	2531	4.4	1722	4.12	6.35
OPX SDM N.7, heated 47.66 h at 900 °C	2583	1.5	1912	9.49	10.91

Note: in space group $P2_1ca$, R_{sym} refers to the agreement among the intensities of the equivalent reflections hkl, $\bar{h}kl$, $h\bar{k}l$, and $\bar{h}\bar{k}l$. $R_{sym} = \Sigma_{hkl}(I_{hkl} - \bar{I})/\Sigma_{hkl}\bar{I}$, where $\bar{I} = (I_{hkl} + I_{\bar{h}kl} + I_{h\bar{k}l}) + I_{\bar{h}\bar{k}l})/4$. In space groups $P12_1/c1$ and $P112_1/a$, R_{sym} refers to the agreement among the intensities of the equivalent reflections hkl and $h\bar{k}l$. $R_{sym} = \Sigma_{hkl}(I_{hkl} - \bar{I})/\Sigma_{hkl}\bar{I}$, where $\bar{I} = (I_{hkl} + I_{h\bar{k}l})/2$. I_{obs} = reflections with $I \geq 3\sigma_I$. R_{obs} and R_{tot} are the final conventional discrepancy indices expressed as $\Sigma||F_o| - |F_c||/\Sigma|F_o|$.

Structure refinement in $P12_1/c1$ and $P112_1/a$

A careful analysis of the Laue symmetry showed that $I_{hkl} \cong I_{h\bar{k}l} \neq I_{\bar{h}kl} \cong I_{\bar{h}\bar{k}l}$, thus indicating a monoclinic symmetry $2/m$ rather than orthorhombic symmetry mmm. In monoclinic Laue symmetry, the calculated discrepancy index R_{sym} between all equivalent reflections improves from 6.3 to 4.4% for Opx SDM N.13 and from 7.1 to 1.6% for Opx SDM N.7. Therefore, structure refinements were performed in monoclinic space groups $P12_1/c1$ and $P112_1/a$, which are subgroups of *Pbca*. The same cell origin was used and independent atoms were taken as those with coordinates x,y,z and $\frac{1}{2} + x, \frac{1}{2} - y, \bar{z}$, which are equivalent in *Pbca* space group. Least-squares refinements were performed using the same procedures as in $P2_1ca$. For both space groups the results were unsatisfactory, as shown by the significant increase of the residual indices R_{obs} (Table 9). Notwithstanding the apparent Laue symmetry, the hypothesis of monoclinic symmetry is unacceptable.

Discussion

The results of the structure refinements do not support the assumption of lower symmetry for the Serra de Magé orthopyroxene. On the other hand, violation of extinction conditions of *Pbca* symmetry and the monoclinic symmetry equivalence of the reflections are unquestionable. Therefore, the alternative interpretations proposed by Sasaki et al. (1984) must be considered.

TABLE 10. *Pbca* forbidden reflections, *C2/c* superimposed reflections, observed and calculated structure factors, and approximate evaluation of the augite content

Pbca forbidden refl.	*C2/c* refl.	F_c (augite)	OPX SDM N.13 I/σ_I	OPX SDM N.13 F_o**	OPX SDM N.13 F_o/F_c	OPX SDM N.13 $100(F_o)^2/(2F_c)^2$ = % augite	OPX SDM N.7 I/σ_I	OPX SDM N.7 F_o**	OPX SDM N.7 F_o/F_c	OPX SDM N.7 $100(F_o)^2/(2F_c)^2$ = % augite
032	$\bar{1}32$	56.5	11	23.8	0.42	4.4	75	40.7	0.72	12.9
052	$\bar{1}52$	15.8	5	7.5	0.47	5.6	17	11.7	0.74	13.7
072	$\bar{1}72$	35.5	6	13.0	0.37	3.4	16	23.3	0.66	10.8
016	$\bar{3}16$	38.6	4	14.3	0.37	3.4	18	25.9	0.67	11.3
056	$\bar{3}56$	84.6	26	33.1	0.39	3.8	66	59.5	0.70	12.4

* Transformation matrix $hkl_{Pbca} \rightarrow hkl_{C2/c}$: ½ 0 −½
0 1 0
0 0 1.

** Scale factor from *Pbca* structure refinement.

The $0kl$ forbidden reflections occurring in X-ray single-crystal diffraction data of the two Serra de Magé orthopyroxenes have $k = 2n + 1$ and $l = 4n + 2$. As already noted by Sasaki et al. (1984), they are consistent with reflections from *C2/c* clinopyroxene exsolved on (100) and superimposed on the $0kl$ forbidden reflections of the orthopyroxene. This requires that the orientation of the monoclinic cell, with respect to the orthorhombic cell, is $\mathbf{a}^*_{Aug} \equiv \mathbf{a}^*_{Opx}$, $\mathbf{c}^*_{Aug} \equiv [101]^*_{Opx}$, and $\mathbf{b}^*_{Aug} \equiv \mathbf{b}^*_{Opx}$, which is exactly that found in this study by TEM analysis. With this orientation, all diffraction effects of monoclinic *C2/c* augite are superimposed on those of *Pbca* orthopyroxene with $(h + l) = 2n$. This overlap explains the monoclinic-like equivalence of the collected reflections. In fact, considering the transformation matrix $hkl_{Pbca} \rightarrow hkl_{C2/c}$ (Table 10), four equivalent reflections of orthopyroxene with $(h + l) = 2n$ overlap with two different pairs of monoclinic equivalent reflections: hkl_{Pbca} and $h\bar{k}l_{Pbca}$ are overlapped by $h'kl_{C2/c}$ and $h'\bar{k}l_{C2/c}$, and $\bar{h}kl_{Pbca}$ and $\bar{h}\bar{k}l_{Pbca}$ are overlapped by $h''kl_{C2/c}$ and $h''\bar{k}l_{C2/c}$, where $h' = (h/2 - l/2) \neq h'' = (-h/2 - l/2)$.

In Table 10, we report the indices of the observed $0kl$ forbidden reflections (with $I \geq \sigma_I$) in *Pbca*, the corresponding indices in the *C2/c* phase, the values of the relevant observed structure factors, F_o, in the scale of the *Pbca* refinement, and the values of the corresponding calculated structure factors, F_c, from a refinement of a *C2/c* augite with the same composition as the (100) lamellae. For the two samples, we calculated the ratio F_o/F_c for all forbidden reflections: in each sample these values are similar, confirming the assumption that the forbidden reflections are due to exsolved *C2/c* pyroxene. An approximate evaluation of the augite content of the samples is obtained from the ratio $100(F_o)^2/(2F_c)^2$, where the calculated structure factor for the augite is doubled to take into account the volume of the orthorhombic cell with respect to the monoclinic cell. The augite content of the two crystals is about 4 and 12%, respectively, indicating that the exsolved *C2/c* phase is not homogeneously distributed in different orthopyroxene crystals.

The results of this study allow us to formulate the following conclusions: (1) The *Pbca* space group for the Serra de Magé orthopyroxene is confirmed; the hypothesis of $P2_1ca$ or lower symmetry must be rejected. (2) Violations of extinction conditions for *Pbca* symmetry as well as the monoclinic Laue symmetry $2/m$ exhibited by the reflections are explained by the presence of an exsolved *C2/c* augite phase. (3) An approximate estimation of the amount of monoclinic phase present is obtained from the ratio of observed to calculated structure factors. (4) A simultaneous structure refinement of both *Pbca* and *C2/c* phases (work in progress) should permit the subtraction of the contribution of the superimposed reflections of the augite from the F_o of the orthopyroxene. In this way, it should be possible to refine more correctly the *Pbca* phase and to obtain an accurate estimate of the content of the *C2/c* phase.

ACKNOWLEDGMENTS

The authors thank G.P. Sighinolfi, who kindly supplied the Serra de Magé meteorite sample. Financial support was provided by the CNR (Centro di Studio per la Cristallochimica e la Cristallografia, Pavia; Centro di Studio sui Problemi dell'Orogeno delle Alpi Orientali, Padua), and MURST (grants 60% G.M.M. and 40% E. Bruno). The manuscript benefited from the informal review of F. Hawthorne and from the formal reviews of A.J. Brearley, H. Takeda, G. Harlow, and an anonymous reviewer.

REFERENCES CITED

Blessing, R.H., Coppens, P., and Becker, P. (1974) Computer analysis of step-scanned X-ray data. Journal of Applied Crystallography, 7, 488–492.

Busing, W.R., Martin, K.O., and Levy, H.S. (1962) ORFLS, a Fortran crystallographic least-squares program. U.S. National Technical Information Service, ORNL-TM-305.

Cannillo, E., Germani, G., and Mazzi, F. (1983) New crystallographic software for Philips PW 1100 single crystal diffractometer. CNR Centro di Studio per la Cristallografia, Internal Report 2.

Domeneghetti, M.C., Molin, G.M., and Tazzoli, V. (1995) A crystal-chemical model for *Pbca* orthopyroxene. American Mineralogist, 80, 253–267.

Hamilton, W.C. (1965) Significance test on the crystallographic R factor. Acta Crystallographica, 18, 502.

Harlow, G.E., Nehru, C.E., Prinz, M., Taylor, G.J., and Keil, K. (1979) Pyroxenes in Serra de Magé: Cooling history in comparison with Moama and Moore County. Earth and Planetary Science Letters, 43, 173–181.

Ibers, J.A., and Hamilton, W.C., Eds. (1974) International tables for X-ray crystallography, vol. 4, p. 99–101. Kynoch, Birmingham, U.K.

Lehmann, M.S., and Larsen, F.K. (1974) A method for location of the peaks in step-scan measured Bragg reflections. Acta Crystallographica, A30, 580–584.

Luo, G., Xue, J., Xu, H., Xu, H., and Hu, M. (1992) Confirmation of the terrestrial occurrence of orthopyroxene with space group $P2_1ca$. American Mineralogist, 77, 115–120.

North, A.C.T., Phillips, D.C., and Mathews, F.S. (1968) A semi-empirical method of absorption correction. Acta Crystallographica, A24, 351–359.

Sasaki, S., Prewitt, C.T., and Harlow, G.E. (1984) Alternative interpretation of diffraction patterns attributed to low ($P2_1ca$) orthopyroxene. American Mineralogist, 69, 1082–1089.

Smyth, J.R. (1974) Low orthopyroxene from a lunar deep crustal rock: A new pyroxene polymorph of space group $P2_1ca$. Geophysical Research Letters, 1, 27–29.

——— (1975) Intracrystalline cation order in a lunar crustal troctolite. Proceedings of the Sixth Lunar Science Conference, 821–832.

Steele, I.M. (1975) Mineralogy of lunar norite 78235: Second lunar occurrence of $P2_1ca$ pyroxene from Apollo 17 soils. American Mineralogist, 60, 1086–1091.

Tokonami, M. (1965) Atomic scattering factors for O^{2-}. Acta Crystallographica, 19, 486.

Manuscript received December 9, 1994
Manuscript accepted May 16, 1995